Green Chemistry

PAPER

View Article Online
View Journal | View Issue

Cite this: *Green Chem.*, 2021, **23**, 7751

Adjusting SiO_2 : C mole ratios in rice hull ash (RHA) to control carbothermal reduction to nano-structured SiC, Si_3N_4 or Si_2N_2O composites†

Mengjie Yu,[a] Eleni Temeche,[b] Sylvio Indris [c] and Richard M. Laine *[a,b]

Received 11th June 2021,
Accepted 8th September 2021

DOI: 10.1039/d1gc02084f

rsc.li/greenchem

We report here extracting SiO_2 as spirosiloxane $[(CH_3)_2C(O)CH_2CH(O)CH_3]_2Si$ from rice hull ash (RHA) to carefully control the SiO_2 : C mole ratios, allowing direct carbothermal reduction to SiC, Si_3N_4, or Si_2N_2O without the need to add extra carbon and as a mechanism to preserve the original nanocomposite structure. We can adjust SiO_2 : C ratios from 2 : 15 to 13 : 35 simply by reacting RHA with hexylene glycol (HG) with catalytic base to distillatively extract SiO_2 to produce silica depleted RHA (SDRHA) with SiO_2 contents of 40–65 wt% and corresponding carbon contents of 60–35 wt% with specific surface areas (SSAs) of >400 $m^2\ g^{-1}$. On heating $SDRHA_{40-65}$ at 1400–1500 °C in an Ar, N_2, or N_2–H_2 atmosphere, XRD patterns reveal formation of SiC, Si_3N_4, or Si_2N_2O as the major phase with some residual hard carbon. SEM studies reveal mixtures of particles and whiskers in the products, which show BET specific surface areas >40 $m^2\ g^{-1}$ after oxidative removal of excess carbon. Dilute acid and boiling water prewashing of RHA with milling eliminates typical product impurities compared to those found using conventional carbothermal reduction of agricultural wastes, which qualifies the resulting composites as components for electrochemical energy storage devices among other applications, to be reported elsewhere.

Introduction

Commercially, most silicon carbide (SiC) and silicon nitride (Si_3N_4) production uses conventional carbothermal reduction or nitridation of SiO_2 by heating mixtures of quartz sand and carbon at >1900 °C.[1–3] Select efforts have explored replacing these starting materials with waste products, including natural sources such as rice husk and biomass,[4–7] and obsolete electrical appliances.[8,9] These sources can provide large quantities of SiO_2 or carbon, from which nanoscale reactants can be obtained by pre-treatment. As such, waste starting materials for fabricating SiC and Si_3N_4 may offer several advantages: (1) the environmental benefits related to a reduced carbon footprint; (2) the economical disposal of waste materials; (3) improved properties arising from reduction of product particle sizes enabled by initiating production using nanoscale mixtures; and (4) economization of energy and capital equipment costs due to decreases in processing temperatures and times, *etc.*[4,10–13]

Rice is the second most-consumed food globally and is usually distributed in the market after polishing to remove rice hulls (RHs), which make up ~20 wt% of as grown rice. RHs are generally considered agricultural waste since they have no obvious direct commercial uses. However, the discovery that they consist of 15–20 wt% amorphous SiO_2 led to extensive efforts to produce SiC and Si_3N_4 whiskers and particles.[14–16]

Lee and Cutler first used RHs to produce SiC in 1975.[2] Thereafter, a number of groups explored transforming RHs to SiC by heating at 1200–1500 °C under inert or reducing atmospheres.[10,17,18] In typical processes, RHs are first coked or ashed prior to conversion to SiC or Si_3N_4. Gorthy *et al.*[19] describe combusting RHs at 280 °C in air to produce black ash with ~45 wt% SiO_2. Then, heating to 1500 °C/Ar converts this ash to SiC whiskers (20 vol%) 0.1–0.11 μm diameters and 6–14 μm particles (80 vol%). Li *et al.*[18] heated RHs at 700 °C/Ar, then used microwave heating to generate 100–200 nm diameter whiskers and 60–130 nm particles. Similarly, Sujirote *et al.*[20] charred RHs at 1000 °C/Ar and then at 1500 °C/Ar producing SiC whisker and particle mixtures with 0.1–1 μm diameters.

However, commercial manufacture of SiC and Si_3N_4 from RHs has yet to be realized. Most RHs are disposed by burning, generating rice hull ash (RHA) used primarily to enrich soil to

[a]*Macromolecular Science and Engineering, University of Michigan, Ann Arbor, MI 48109, USA*
[b]*Department of Materials Science and Engineering, University of Michigan, Ann Arbor, MI 48109, USA. E-mail: talsdad@umich.edu*
[c]*Institute for Applied Materials-Energy Storage Systems (IAM-ESS), Karlsruhe Institute of Technology (KIT) Eggenstein-Leopoldshafen 76344, Germany*

†Electronic supplementary information (ESI) available. See DOI: 10.1039/d1gc02084f

fertilize crops grown the next season.[1,21,22] The quantities of RH derived SiO_2, carbon, and residual mineral content vary depending on crop variety, growth climate, and location,[23,24] as well as the temperature and duration of combustion. Yeoh *et al.*[25] reported that amorphous SiO_2 remained at combustion temperatures up to 900 °C for <1 h, while crystalline SiO_2 formed at 1000 °C rapidly in 5 min. Hwang *et al.*[26] found greater SiO_2 percentages in RHA and more volatile alkaline components at higher combustion temperatures.

Generally, RHA contains 80–90 wt% amorphous SiO_2, while carbon and trace amounts of alkaline elements such as K, S, Ca, Mg comprise the remaining mass. Given the relatively high SiO_2 content, only a limited number of studies report the synthesis of SiC and Si_3N_4 from RHA.[13,20,27,28] Those reports, typically use RHA as the SiO_2 source, adding an external carbon reactant. Thus, Li *et al.*[27] pyrolyzed a phenolic resin carbon source with RHA as a prelude to generating SiC nanowires. The RHA and resin mixture was embedded in graphite and then heated at 1600 °C. Chen *et al.*[28] used a graphene carbon source and template to grow SiC whiskers with diameters of 30–120 nm.

Likewise, excess carbon and coincidentally formed CO gas are essential in carbothermal nitridation producing Si_3N_4.[29–31] Abdulhameed *et al.*[32] combined RHA with sugarcane bagasse ash (carbon source), to synthesize Si_3N_4 by reacting with NH_4OH *via* hydrothermal reaction. In other work, Pavarajarn *et al.*[33] detailed the carbothermal nitridation of RHA as a source of Si_3N_4 fibers and whiskers. Although no extra carbon was added, the employed RHA contained only 45 wt% SiO_2, which is suspected to be a feature originating from the growing environment (Thailand). It is evident that RHA with 80–90 wt% SiO_2 is not a viable starting point for these materials due to its quite low carbon content. However, this SiO_2 : C ratio is rather typical of RHA sources worldwide, suggesting that carbon must be added to adjust stoichiometries that favor the formation of SiC and Si_3N_4. Thus, controlling the SiO_2 : C ratios while retaining the intimately mixed carbon and SiO_2 in the nanoscale is essential for more efficient use of RHA as a starting material for carbothermal reduction.

In addition to the variability of SiO_2 and carbon contents in agricultural waste materials, another barrier hinders the commercial production of SiC and Si_3N_4 from RH and/or RHA. As discussed above, most biomass and agricultural sources frequently contain significant quantities of impurities, closely affecting phases, morphologies, and purities of as-produced products.[12,34]

In light of the above background, the work presented here offers an alternate approach to the synthesis of SiC, Si_3N_4, and Si_2N_2O composites using acid purified RHA. Rather than introducing extra carbon, the ratio of SiO_2 : C is optimized by distillative removal of SiO_2 from RHA generating SDRHA with controllable SiO_2 : C ratios. This process coincidentally and simply eliminates typical impurities providing starting materials especially utile for carbothermal reduction reactions *versus* conventional agricultural sources.

Experimental section

Synthesis of SDRHA

Rice hull ash (RHA) was a gift from Wadham Energy Inc. (Williams, CA). 2-Methyl-2,4-pentanediol (hexylene glycol) was purchased from ARCOS Organic, while potassium hydroxide (KOH) and hydrochloric acid (HCl) were purchased from Sigma-Aldrich (St Louis, MO), of which all were used as received.

The detailed analyses of RHA and impurity removal processes are reported elsewhere.[35] The as-received RHA was first milled in dilute hydrochloric acid (HCl) and repeatedly boiled in DI water to remove impurities. In a 2 L container, RHA (200 g) was milled with 200 g of yttria-stabilized zirconia sphere media (3 mm diameter) in HCl solution (0.1 M). The RHA was milled for 48 h before being recovered by suction filtration through a Buchner funnel, which was then washed with 500 mL DI water. Then, the acid milled RHA was boiled for 24 h and separated by filtrating through a Buchner funnel. The boiling and filter processes were repeated until the pH of boiled water filtered off was neutral. Last, the RHA was dried at 100 °C/vacuum overnight prior to the silica-depleting reaction.

A mixture of 250 mL hexylene glycol (HG) and 4.2 g KOH (75 mmol) was first heated to 190 °C in a 250 mL three-neck flask equipped with a stir bar to remove water for 3 h. Dried RHA powders (~50 g) were added to the HG + KOH solution. The mixture was heated to 200 °C in a pyrex distillation setup. After 100 mL HG was distilled, another 100 mL HG was added. The dissolved SiO_2 content was adjusted by controlling reaction times and HG volumes introduced to the reaction. For instance, after reacting with 100 mL HG in 24 h, SDRHA with ~70 wt% SiO_2 was obtained. When heating is terminated and no more HG is added, the SiO_2:C ratios are fixed in the recovered SDRHA.

Production of SiC, Si_3N_4, and Si_2N_2O composites from SDRHA

SDRHA powder was placed in a graphite crucible and covered with an alumina disk, which was then heated in a tube furnace (GSL-1700X, MTI Corporation). Heat-treatments were conducted at different temperatures and duration times at a heating rate of 10 °C min^{-1}. Heating in atmosphere of Ar, N_2, and N_2–H_2 mixtures generates SiC, Si_3N_4, and Si_2N_2O composites, respectively, with some amounts of excess carbon, crystalline SiO_2 and secondary Si-containing phases of the related compounds. Detailed discussions are found in the result section.

Characterization

Fourier-transform infrared spectroscopy (FTIR). Nicolet 6700 Series FTIR spectrometer (Thermo Fisher Scientific, Inc.) was used to collect FTIR spectra. The samples were mixed with KBr (International Crystal Laboratories). N_2 was purged in the chamber during data acquisition in the range of 4000–400 cm^{-1}.

X-ray diffraction (XRD). Rigaku Miniflex diffractometer (Rigaku Denki., Ltd, Tokyo, Japan) with Cu-Kα radiation (k = 0.154 nm) was used to identify the phases and characterize the crystalline nature of RHA, SDRHA, SiC, Si_3N_4, and Si_2N_2O com-

posites. The diffraction data were recorded in the 2θ over the ranges of 10–80° 2θ using a scan rate of 5 degree min^{-1}. The presence of crystallographic phases and their wt% fraction were refined using PDXL software (version 2.8.4).

BET specific surface area (SSA) analyses. Micromeritics ASAP 2020 sorption analyzer was used to measure the SSAs. Samples were degassed at 300 °C for 6 h prior to analyses by N_2 physisorption at −196 °C (77 K). BET method using 10 data multipoint with relative pressures of 0.05–1 was applied. The pore volume was calculated based on the Barret–Joyner–Halenda (BJH) model.

Scanning electron microscopy (SEM). JSM-IT300HR In Touch Scope SEM (JEOL USA, Inc.) was used to acquire the microstructure images and EDX maps of RHA, SDRHA, SiC, Si_3N_4, and Si_2N_2O composites.

Thermogravimetric analysis (TGA). Q600 simultaneous TGA/DSC (TA Instruments, Inc.) was used to determine the carbon content in RHA, SDRHA, SiC, Si_3N_4, and Si_2N_2O composites. Samples (10–20 mg) were placed in alumina pans and ramped to 600 °C at 10 °C min^{-1} in the presence of air (60 mL min^{-1}). The SiO_2 : C mole ratios of SDRHA are calculated from the molar mass and weight of each component as determined by TGA.

Magic-angle spinning (MAS) nuclear magnetic resonance (NMR) spectroscopy. Bruker Avance 500 MHz spectrometer was used to conduct the solid-state NMR at a magnetic field of 11.7 T (ω = 130.3 MHz). Spinning (30 kHz) was performed in 2.5 mm zirconia rotors. A rotor-synchronized Hahn-echo pulse sequence was applied to acquire the spectra at a $\pi/2$ pulse length of 2.7 μs.

X-ray photoelectron spectroscopy (XPS). Kratos Axis Ultra (Kratos Analytical) was used to analyze the elements present. XPS system at room temperature under 3.1×10^{-8} Pa using monochromatic Al source (14 kV and 8 mA) was used to record the core level atoms. Binding energies of all the elements were calibrated relative to C 1s at 284.8 eV. Data was analyzed using CasaXPS software (version 2.3.22PR1.0).

Results and discussion

Combustion followed by stoichiometric alkali treatment is the most common method of extracting SiO_2 from RHA (1), generating extractable silicates as the product (Scheme 1):[23,36,37]

$$SiO_2\ (RHA) + \text{stoichiometric MOH} \longrightarrow M_2SiO_3$$

Scheme 1 Conventional method of extracting SiO_2 from RHA.

However, this two-step process defeats the original advantage of intimate mixing of nanoscale carbon and SiO_2 that enables low-cost production of SiC and Si_3N_4 from RHA. Furthermore, any trace minerals present in the RHA remain in the SDRHA.

In principle, a more environmentally- and economically-friendly approach should eliminate these trace impurities, adjust the SiO_2 content and limit the alkali metal amounts to reduce their presence as impurities. It is now well understood that milling RHA in dilute acid followed by washing with boiling water provides SDRHA with very low impurity levels to the point where it is now possible to process solar-grade silicon (99.999% pure) from this SDRHA;[35] however, in this previously developed process, carbon had to be added.

Most recently, we have resolved multiple problems of the types noted above by learning to remove SiO_2 from RHA by forming spirosiloxane (SP) per (Scheme 2):[38]

We detailed the isolation and purification of distilled SP recently.[38,39] As water is used to dissolve the distilled HG and to separate it from SP, recycling the HG by removing water further highlights the prominent sustainability of this method, not to mention the low toxicity of HG. In addition, the base used as catalyst likely remains as K_2SiO_3 and can also be recycled.

As just noted, SDRHA is a practical precursor to solar grade silicon (99.999% pure).[35] Coincidentally, SP offers access to high surface area fumed SiO_2 and precipitated SiO_2 for vacuum insulation panels.[40] Recently, its utility was extended to high-performance electrodes for hybrid Li^+ supercapacitors[41] and precursors for solid electrolytes.[39]

Synthesis of SDRHA

The as-received RHA used contains ~90 wt% SiO_2. Detailed SDRHA synthesis procedures are reported elsewhere and discussed in the Experimental section.[42] Briefly, the first step is to mill the as-received RHA in dilute acid followed by washing with boiling water, which removes the majority of the mineral impurities.[43,44] The dried RHA is reacted with hexylene glycol using catalytic amounts of potassium hydroxide (Scheme 2), followed by washing to separate SDRHA. Fig. 1a provides representative TGAs of acid-washed/dried RHA and SDRHA at 25–600 °C under air after distilling part, providing respective SiO_2 contents. No apparent mass decrease is observed after oxidation of carbon finishes at ~480 °C, suggesting 60 wt% SiO_2 remains in the $SDRHA_{60}$. Signature peaks for C 1s, Si 2s, Si 2p, and O 1s are shown in the XPS wide survey spectra of

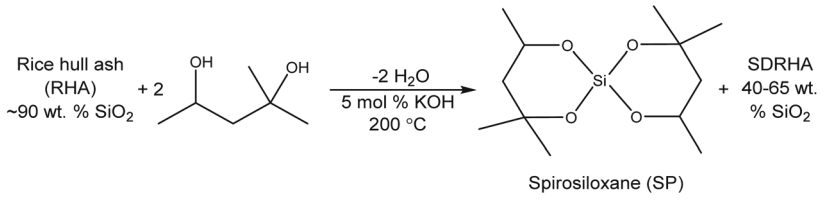

Scheme 2 Dissolution of SiO_2 from RHA allows distillative removal *via* spirosiloxane.

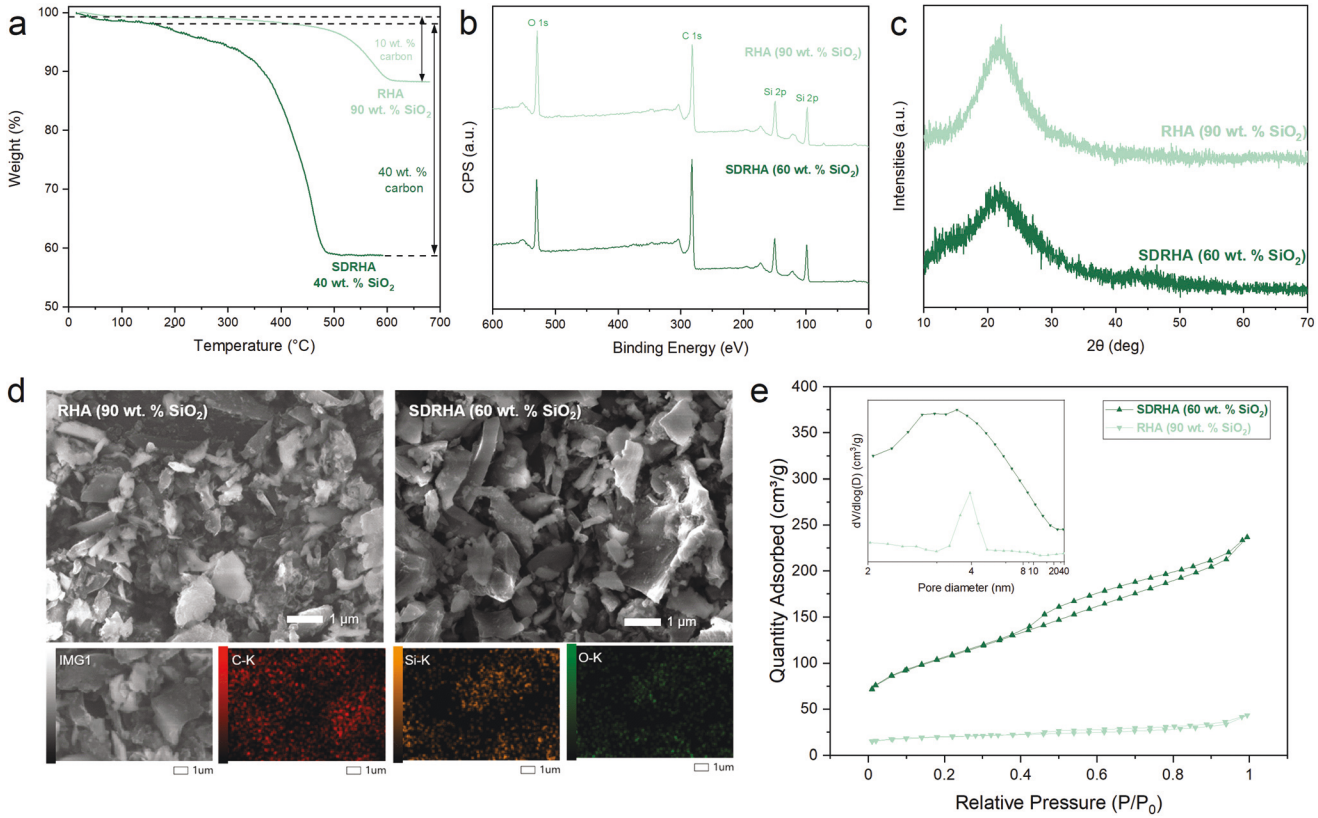

Fig. 1 (a) TGA, (b) XPS survey scan, (c) XRD, (d) SEM images (EDX maps for $SDRHA_{60}$), and (e) N_2 adsorption–desorption isothermal plots and pore size distribution (inset) of RHA and $SDRHA_{60}$.

$SDRHA_{60}$ in Fig. 1b, indicating the removal of impurities from the raw materials.

The XRD patterns shown in Fig. 1c indicate that RHA consists of amorphous SiO_2 and carbon before and after SiO_2 extraction, while EDX analyses (Fig. 1d) confirm intimate mixing of SiO_2 and carbon in SDRHA (60 wt% SiO_2, denoted $SDRHA_{60}$) at nanoscales. As such, the essential conditions for effective carbothermal reduction at relatively low temperatures, *i.e.* milling of amorphous SiO_2 and carbon sources in traditional manufacturing processes,[23,45,46] are met without extra effort.

The SEM images (Fig. 1d) reveal that RHA morphologies are retained in the $SDRHA_{60}$, where the majority of particles range from 1 to 10 μm. Moreover, the SiO_2 and carbon particles are mixed in a porous network, as visualized in the SEM images and attested to by BET measurements. The BJH adsorption cumulative pore volume increases from ~0.05 $cm^3\ g^{-1}$ for RHA to ~0.3 $cm^3\ g^{-1}$ for $SDRHA_{60}$. The pore size distributions in RHA and $SDRHA_{60}$ are illustrated in the inset of Fig. 1e, where broader distributions of pores in the range of 2–4 nm are present in $SDRHA_{60}$. The BET SSAs increase from ~70 $m^2\ g^{-1}$ for RHA to ~345 $m^2\ g^{-1}$ for $SDRHA_{60}$, while those for $SDRHA_{40,50,55,65}$ are ~440, ~420, ~370, and ~220 $m^2\ g^{-1}$. As seen in the N_2 adsorption–desorption isotherms of RHA and $SDRHA_{60}$, the plot characteristics correspond to type IV with H3 hysteresis in IUPAC classifications, which presumably arises from the porous network in non-rigid aggregates of plate-like particles.[47] The enhanced pore volumes and SSAs likely facilitate interactions between SiO_2 and carbon particles and CO and SiO during carbothermal reductions.

Nanocomposites from SDRHA *via* carbothermal reduction

In traditional carbothermal reduction, it is necessary to mill the SiO_2 source with the carbon source as a first step. In contrast, $SDRHA_{40–65}$ consist of SiO_2/C nanocomposites as recovered from distillative removal of SiO_2. Thus, they can be heated directly. Fig. 2a and b present XRDs of SiC derived from heating $SDRHA_{60}$ at 1400–1500 °C under Ar for 8 h (denoted as 1400–1500 °C/Ar per 8 h below), and at 1500 °C for 2–7 h. The corresponding crystalline phases are listed in Table 1, determined using the reference intensity ratio method.

Peaks at 36°, 42°, 60°, and 72° 2θ are associated with the (111), (200), (220), and (311) planes of β-SiC, respectively (3C-SiC, PDF 01-073-1708). The weak shoulders at 33.5° correspond to stacking faults.[48–50] On heating to 1430 and 1450 °C, peaks indexed to the (101) plane of cristobalite at 22° 2θ appear, corresponding to ~20 and 5 wt% cristobalite in the products, respectively. No cristobalite or other SiO_2 phase are observed for reaction times >5 h. Limiting heat-treatment to 4 h gives SiC as the major product with ~3 wt% cristobalite.

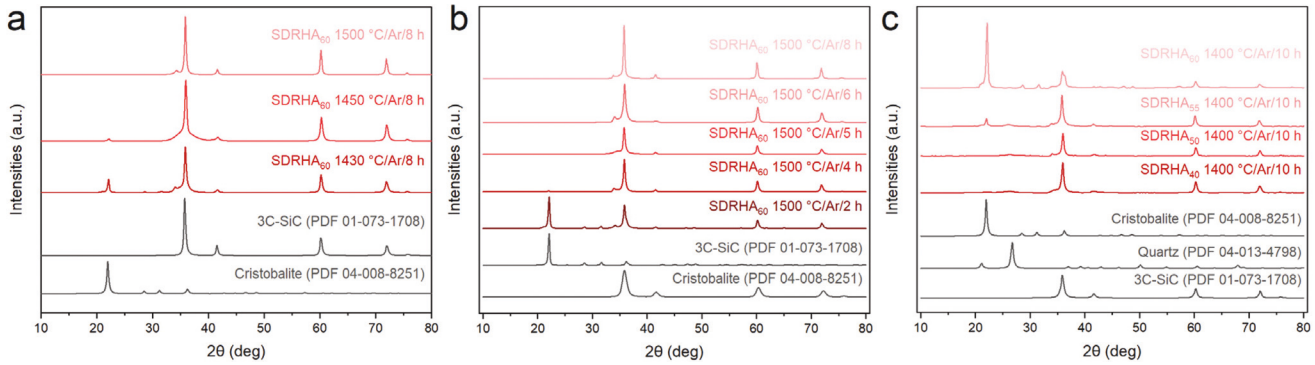

Fig. 2 XRDs from heating (a) $SDRHA_{60}$ at 1430–1500 °C per 8 h/Ar, (b) $SDRHA_{60}$ at 1500 °C for various times, (c) $SDRHA_{40-60}$ at 1400 °C per 10 h/Ar.

Table 1 Crystalline phases of products[a] from heating $SDRHA_{60}$ at 1400–1500 °C/Ar

$SDRHA_{60}$	1430 °C per 8 h	1450 °C per 8 h	1500 °C per 2 h	1500 °C per 4 h	1500 °C per >5 h
SiC	80%	95%	57%	98%	100%
Cristobalite	20%	5%	43%	2%	0%

[a] As-produced composites contain amorphous hard carbon (13.7 ± 0.9 wt% of the total mass, determined by TGA).

Table 2 Phase compositions of products from heating $SDRHA_{40-60}$ at 1400 °C per 10 h/Ar

1400 °C/Ar per 10 h				
Starting material	$SDRHA_{40}$	$SDRHA_{50}$	$SDRHA_{55}$	$SDRHA_{60}$
SiC	88%	79%	74%	16%
Cristobalite	3%	2%	7%	82%
Quartz	9%	19%	20%	2%
Amorphous carbon[a]	34%	22%	20%	10%

[a] Amorphous hard carbon contents are out of the total mass of the as-produced (determined by TGA).

Known reactions involved in the carbothermal reductive synthesis of SiC are:[6,51,52]

$$SiO_2\ (s) + C\ (s) \rightarrow SiO\ (g) + CO\ (g) \quad (1)$$

$$SiO\ (g) + 3CO\ (g) \rightarrow SiC\ (s) + 2CO_2\ (g) \quad (2)$$

$$SiO\ (g) + 2C\ (s) \rightarrow SiC\ (s) + CO\ (g) \quad (3)$$

$$CO_2\ (g) + C\ (s) \rightarrow 2CO\ (g) \quad (4)$$

Previous studies proposed that temperatures lower than 1400 °C were unfavorable for carbothermal reduction and nitridation of RHA.[33] Possible explanations for this observation include rapid SiO_2 losses as gaseous SiO at temperatures ≤1400 °C and dominant solid–solid reactions occurred between SiO_2 and carbon particle contact points (in micron scale mixtures) at temperatures ≤1400 °C.[53–57] Consequently, formation and coincident loss of CO suppresses further SiC formation. The effects of SiO_2 : C ratios are more critical for larger particle sizes.

Conventional carbothermal reduction requires excess carbon to promote complete transformation of SiO_2 to SiC.[2,58,59] The corresponding mole ratios of SiO_2 : C require greater carbon contents than a 1 : 3 stoichiometric ratio. $SDRHA_{40,50,55,60}$ materials offer SiO_2 : C mole ratios of 2 : 15, 1 : 5, 11 : 45, and 3 : 10, respectively, satisfying the excess carbon criterion.

As shown in Fig. 2c, heating $SDRHA_{40,50}$ at 1400 °C for 10 h results in the formation of ~88 and 79 wt% SiC, respectively, while $SDRHA_{60}$ gives ~16 wt% (Table 2). The trend that more carbon in the starting materials leads to a higher proportion of SiC in the products agrees with studies reported earlier that surplus carbon facilitates increases in SiC yields. It is also in keeping with reaction kinetics, wherein higher concentrations of a given reactant will drive a given reaction faster.

The detection of two crystalline SiO_2 phases in products heated at 1400 °C suggests incomplete transformation from quartz to cristobalite, which is reported to occur over the temperature interval of 1100–1400 °C.[60–62] In addition, it is well known that carbon reduces of SiO_2 to SiO; thereby initiating vapor–vapor reactions between SiO and C/CO rather than solid-state reactions alone and leads to lower SiC formation temperatures.[63] All these factors define the trend shown in Table 2, where higher SiC yields result from higher initial carbon contents. The residual hard carbon is easily removed oxidatively at 600 °C or can be part of an SiC/C anode in beyond Li^+ batteries, as will be reported at a later date.

XRD analyses of $SDRHA_{60}$ heated under N_2 confirm formation of α-Si_3N_4 (Fig. 3a and b) per:

$$3SiO_2\ (s) + 6C\ (s) + 2N_2\ (g) \rightarrow Si_3N_4\ (s) + 6CO\ (g) \quad (5)$$

$$3SiO\ (g) + 3C\ (s) + 2N_2\ (g) \rightarrow Si_3N_4\ (s) + 3CO\ (g) \quad (6)$$

No significant peak attributable to SiO_2 or SiC is observed, as commonly found in Si_3N_4 produced by carbothermal nitridation, indicating complete nitridation of SiO_2 under the conditions employed.[29,31] Meanwhile, SiO_2 : C ratios significantly

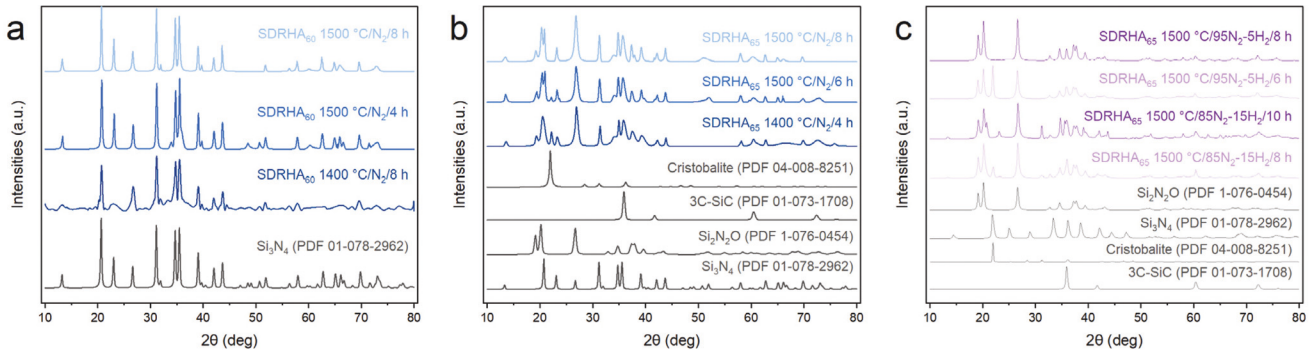

Fig. 3 XRDs from heating (a) $SDRHA_{60}$ at 1400 per 8 h/N_2, 1500 °C per 4 h/N_2, 1500 °C per 8 h/N_2, $SDRHA_{65}$ at 1500 °C under (b) N_2 and (c) N_2–H_2 with different ratios (95–5 and 85–15) for various times.

impact the reaction. $SDRHA_{60}$ provides a mole ratio higher than the stoichiometric SiO_2 : C ratio of 1 : 2 for carbonitriding of SiO_2, resulting in ~24 wt% residual carbon in the products, as discussed below. XRDs in Fig. 3b indicate that products derived from $SDRHA_{65}$ (SiO_2 : C mole ratio = 13 : 35) consist of Si_3N_4, Si_2N_2O, SiC, and cristobalite (Table 3) as well as residual hard carbon. The relative Si_3N_4 and SiC compositions correlate with the secondary reaction:

$$3SiC\ (s) + 2N_2\ (g) \rightarrow Si_3N_4\ (s) + 3C\ (s) \quad (7)$$

Peak intensities indexed to cristobalite at 22° 2θ decrease at longer heating times, becoming negligible after 8 h.

Silicon oxynitride (Si_2N_2O), a refractory material with high chemical and oxidation resistance, is a non-negligible phase produced during carbothermal nitridation $SDRHA_{65}$. Gundiah *et al.*[64] obtained Si_2N_2O nanowires (dia. ~300 nm) by reacting silica gel with carbon nanotubes at 1360 °C/4 h/NH_3, while longer treatments (≥7 h) generated mainly Si_3N_4 nanowires. Ramesh *et al.*[65] reported that carbothermal reduction and nitridation of amorphous $SiO_{1.7}$ at 1623 K (1350 °C) lead exclusively to formation of Si_2N_2O and reactions of amorphous SiO_2 lead exclusively to the formation of Si_3N_4. Ma *et al.*[66] successfully synthesized Si_2N_2O powders using diatomite and sucrose as silicon and carbon sources *via* carbothermal nitridation with a SiO_2 : C molar ratio of 2 and a temperature of 1550 °C as the optimized parameters. Multiple other groups also report increasing yields of Si_2N_2O on adding catalysts: Y_2O_3,[67,68] Fe,[64] and Fe_2O_3 [69] into mixtures of SiO_2 and carbon. Such catalytic additives can become impurities in the products.

Interestingly, composites with Si_2N_2O as the major phase (>70 wt% of the total mass) were produced by heating SDRHA in an N_2 : H_2 mixture. Theoretically, the stoichiometric SiO_2 : C mole ratio is 2 : 3, per:

$$2SiO_2\ (s) + 3C\ (s) + N_2\ (g) \rightarrow Si_2N_2O\ (s) + 3CO\ (g) \quad (7)$$

$SDRHA_{65}$, with a relatively higher SiO_2 : C mole ratio (13 : 35), was chosen to access sufficient oxygen from SiO_2, by which composites with relatively low excess carbon (5.7 ± 0.9 wt%) were obtained. Fig. 3c illustrates representative XRDs of product phases from heating $SDRHA_{65}$ in N_2 : H_2 at $95N_2$: $5H_2$ or $85N_2$: $15H_2$. Similar to the aforementioned Si_3N_4 products, Si_2N_2O, Si_3N_4, SiC, and cristobalite phases are present in the composites (Table 3). With longer heating times, further reduction leads to higher conversions reducing cristobalite content but coincidentally generating more Si_3N_4, as prolonged treatment times will result in further reduction of oxygen in Si_2N_2O, forming Si_3N_4:

$$3Si_2N_2O\ (s) + 3C\ (s) + N_2\ (g) \rightarrow 2Si_3N_4\ (s) + 3CO\ (g) \quad (8)$$

Addition of H_2 in the systems leads to lower N_2 partial pressures and consequently lower Si_3N_4 yields,[70] while the presence of H_2 affects the carbonitriding mechanisms by both direct and indirect reduction of SiO_2 per:

$$SiO_2\ (s) + H_2\ (g) \rightarrow SiO\ (g) + H_2O\ (g) \quad (9)$$

$$C\ (s) + 2H_2\ (g) \rightarrow CH_2\ (g) \quad (10)$$

$$H_2O\ (g) + C\ (s) \rightarrow H_2\ (g) + CO\ (g) \quad (11)$$

$$SiO_2\ (s) + CH_4\ (g) \rightarrow SiO\ (g) + CO + 2H_2\ (g) \quad (12)$$

Fig. 4a and b illustrate TGAs of representative products derived from carbothermal reduction of SDRHA with SiC and

Table 3 Crystalline phase compositions from heating $SDRHA_{65}$ at 1500 °C for various times under N_2 or N_2–H_2 with different ratios (95/5 and 85/15)

$SDRHA_{65}$							
Temperature	1500 °C						
Atmosphere	N_2			$95N_2$–$5H_2$		$85N_2$–$15H_2$	
Duration	4 h	6 h	8 h	6 h	8 h	8 h	10 h
Si_2N_2O	32%	33%	36%	74%	84%	70%	88%
Si_3N_4	38%	50%	58%	5%	<1%	12%	5%
SiC	26%	15%	36%	2%	6%	14%	2%
Cristobalite	4%	2%	6%	19%	<1%	4%	5%
Amorphous carbon[a]	15.3 ± 1.1%			5.7 ± 0.9%			

[a] Amorphous hard carbon contents from total mass of as-produced material (determined by TGA).

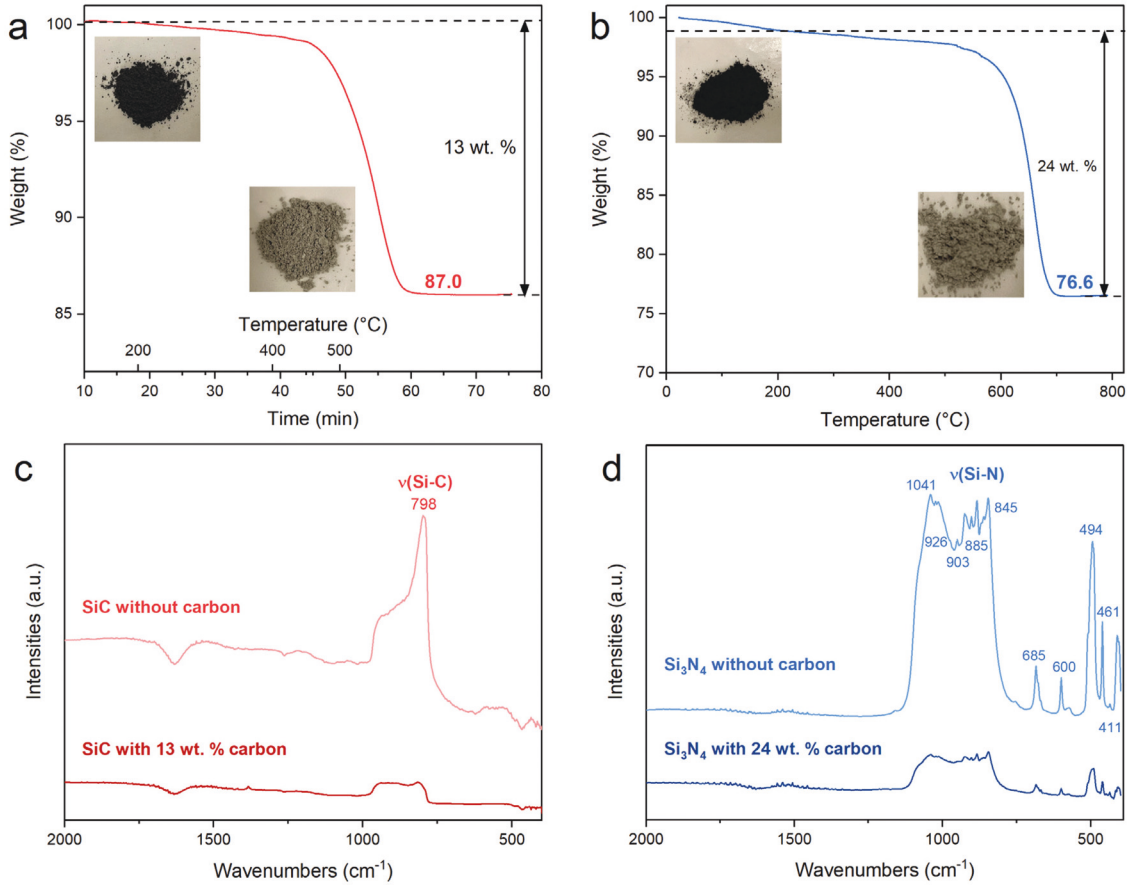

Fig. 4 Representative TGA curves and optical images of (a) SiC, (b) Si_3N_4, and FTIR spectra of (c) SiC, (d) Si_3N_4 composites with and without carbon.

Si_3N_4 as the major phase, indicating excess carbon remains in all systems when heated to 1500 °C. Thus, ~13 wt% unreacted carbon remains in SiC, whereas as-produced Si_3N_4 retains ~24 wt% carbon. The resulting composite powders appear as dark grey due to mixed with excess carbon, which shows light grey green after oxidative removal of residual carbon, the typical color of SiC and Si_3N_4 produced in conventional manufacturing. Given that less carbon is involved in the starting $SDRHA_{65}$ for synthesizing Si_2N_2O and more carbon is consumed by reacting with H_2, a lower amount of excess carbon is found in the composites (5.7 ± 0.9 wt%) than in the former two systems.

The Fig. 4c FTIR of SiC with 13 wt% carbon presents a broad peak from 790 to 1000 cm^{-1} corresponding to the overlap of ν(Si–C) and ν(C–C). After oxidation at 500 °C/O_2/1 h, a strong absorption appears centered at 798 cm^{-1} that can be assigned to ν(Si–C), suggesting the formation of cubic SiC,[71] consistent with the β-SiC phase indexed from XRD results discussed above. The enhanced intensity of ν(Si–C) peak at ~800 cm^{-1} is presumably due to exposure of SiC after removing the excess carbon.

In the spectrum of Si_3N_4 (Fig. 4d), the broad band from 800 to 1100 cm^{-1} reveals an overlap of ν(Si–N) and ν(Si–O) from components including Si_3N_4 and SiO_2 from oxidation of Si_3N_4 particle surfaces.[32] Similar to the SiC product, peak intensities are enhanced on removing excess carbon. The bands at 926, 903, 885, 845, and 685 cm^{-1} are typical for α-Si_3N_4, compatible with XRD results.

In composites with Si_2N_2O as the major phase, the characteristic peaks of Si_2N_2O at 1090, 989, 910, and 679 cm^{-1} are observed (Fig. 5a).[72] An additional band at 850 cm^{-1} is shown in the composites from heating $SDRHA_{65}$ at 1500 °C per 6 h/$95N_2$–$5H_2$, which is attributed to ν(Si–C) and ν(Si–O) from SiC and cristobalite phases in the system.

Fig. 5b presents solid-state ^{29}Si NMR spectra of representative SiC and Si_2N_2O composites derived from SDRHA. The ^{29}Si chemical shift is sensitive to adjacent bonded atoms; thus, small differences in the various polymorphs of one compound can be resolved. The single resonance peak centered at ~ −19 ppm is associated with SiC_4 units in β-SiC, consistent with the XRD discussed above (Fig. 2).[73–75] Typically, broader line widths in solid-state NMR spectra are associated with samples of lower crystallinity. The relatively broad peak is ascribed to some extent to crystalline disorder (*e.g.* twinning, stacking faults), as confirmed by the weak shoulder at ~34° 2θ indexed to stacking faults (Fig. 2).

As for the Si_2N_2O composites from carbonitridation, the ^{29}Si resonance at ~ −61 ppm corresponds to the tetrahedral SiN_3O structural unit in Si_2N_2O.[74] The ^{29}Si resonance peak at ~ −48 ppm is assigned to tetrahedral Si–N in Si_3N_4,[74] while the

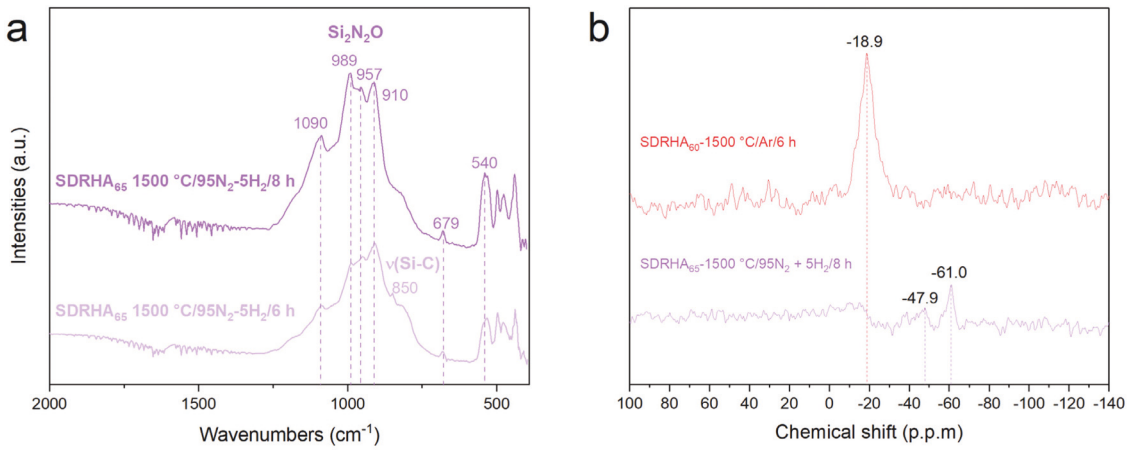

Fig. 5 Representative (a) FTIR spectra of Si_2N_2O composites from different heat treatments, and (b) ^{29}Si NMR of SiC and Si_2N_2O composites.

weak hump at ~ −19 ppm probably arises from nanocrystalline SiC, as identified by XRD (Fig. 3c). However, no peak associated with cristobalite (~ −110 ppm (ref. 76 and 77)) is observed in the spectrum, presumably due to its low content in the sample.

XPS was used to identify the elemental compositions and oxidation states of products with SiC, Si_3N_4, and Si_2N_2O as the major phase. The survey scans of all composites show signature peaks associated with corresponding elements, where no impurities are detected (Fig. S1†). The representative XPS spectra shown in Fig. 6a and Fig. S2† correspond to products from $SDRHA_{60}$ heated at 1500 °C per 8 h before and after oxidative removal of carbon, respectively. Both of the Si 2s and Si 2p spectra in Fig. S2† exhibit one single peak associated with the Si^{4+} state in SiC composites.[78–80]

Deconvolution of the Si 2p region reveals peaks at 101.7 eV for Si–C bonds, while a second peak at 102.5 eV originates from the incorporation of oxygen, resulting in a shift to higher binding energy. In comparison, the Si 2p double peaks at ~101 and ~103.1 eV for Si–C and Si–O bonds, respectively, are observed in the spectra collected from the SiC sample following oxidative removal of carbon.[81,82] The most easily oxidized SiC surface, the SiC whiskers most likely provide the distinct Si–O peaks derived from surface oxidation during oxidative removal of carbon.[79] The C 1s spectra of SiC before and after removing carbon are both fitted with four Gaussian peaks, while the peak at ~283.5 eV indexed to Si–C bonds is more evident in spectra taken after removal of carbon. Intense peaks ascribed to C–C bonds (285.2–285.6 eV), and two other components associated with C–O (287.1 eV) and C═O bonds (289.5 eV) originate from the residual hard carbon.[83,84]

As for the Si_3N_4, from heating $SDRHA_{60}$ at 1500 °C per 8 h/N_2 (Fig. 6b), peak fitting in the Si 2p region reveals an intense peak at 101.8 eV attributed to Si_3N_4.[82] The component at 102.8 eV is assigned to Si–O bonds when the Si atoms bonded to both N and O, as the Si–O bonds originate from oxidation during carbon removal. The intense peak located at 398.1 eV in the N 1s spectra is assigned to N–Si bonds in Si_3N_4, while N–O bonds correspond to the weak peak at 399.4 eV.[85–87]

In comparison, the Si 2p spectra of the Si_2N_2O composite ($SDRHA_{65}$-1500 °C per 8 h/95N_2–5H_2) shown in Fig. 6c consist of three fitted peaks. The two peaks located at 103.2 eV and 102.2 eV are attributed to Si–O and Si–N–O bonds,[88,89] respectively, where the shifts compared to Si–O bonds in SiO_2 and Si–N bonds in Si_3N_4 are typical for Si_2N_2O.[90] Si–C bonds of SiC in the composites show another peak at 101.1 eV, consistent with analyses from XRD. Meanwhile, peaks at 398.4 eV and 397.2 eV in the N 1s spectra can be assigned to N–Si–O bonds and N–O bonds within the Si_2N_2O structure.

SEM and EDX images in Fig. 7 were obtained from the oxidized samples, revealing cylindrical morphologies. SiC particles with sizes ranging between 10 and 200 nm can be observed among SiC whiskers with diameters of 100–140 nm and lengths up to 5 μm. EDS maps show well-distributed Si and C elements. Oxygen was also detected after oxidative carbon removal, as discussed above.

The proposed SiC whisker growth mechanisms focus on heterogeneous vapor–liquid–solid, birth-and-spread growth, vapor–vapor growth.[91,92] Nucleation and growth of SiC whiskers are believed to result mainly from gas-phase reactions between SiO and CO.[93] Although the formation and growth of SiC polymorphs are not fully understood as yet, it is widely accepted that additives, starting materials, impurities, and growth conditions all affect the crystallization kinetics of SiC and the subsequent differences in polymorphs and phases.[10,93,94] Similar morphologies are observed in the Si_3N_4 and Si_2N_2O composites (Fig. 7b and c). Irregular aggregates mixed with whiskers with diameters of 100–200 nm predominate and are several microns in length.

The as-synthesized composites show BET SSAs of >150 m^2 g^{-1} with excess hard carbon. Oxidative removal of carbon followed by BET studies were undertaken, by which the N_2 adsorption isotherms for SiC and Si_3N_4 obtained on heating at different temperatures are depicted in Fig. 8a and b. Incremental increases in the measured BET SSAs were observed with lower synthesis temperatures. The BET surface

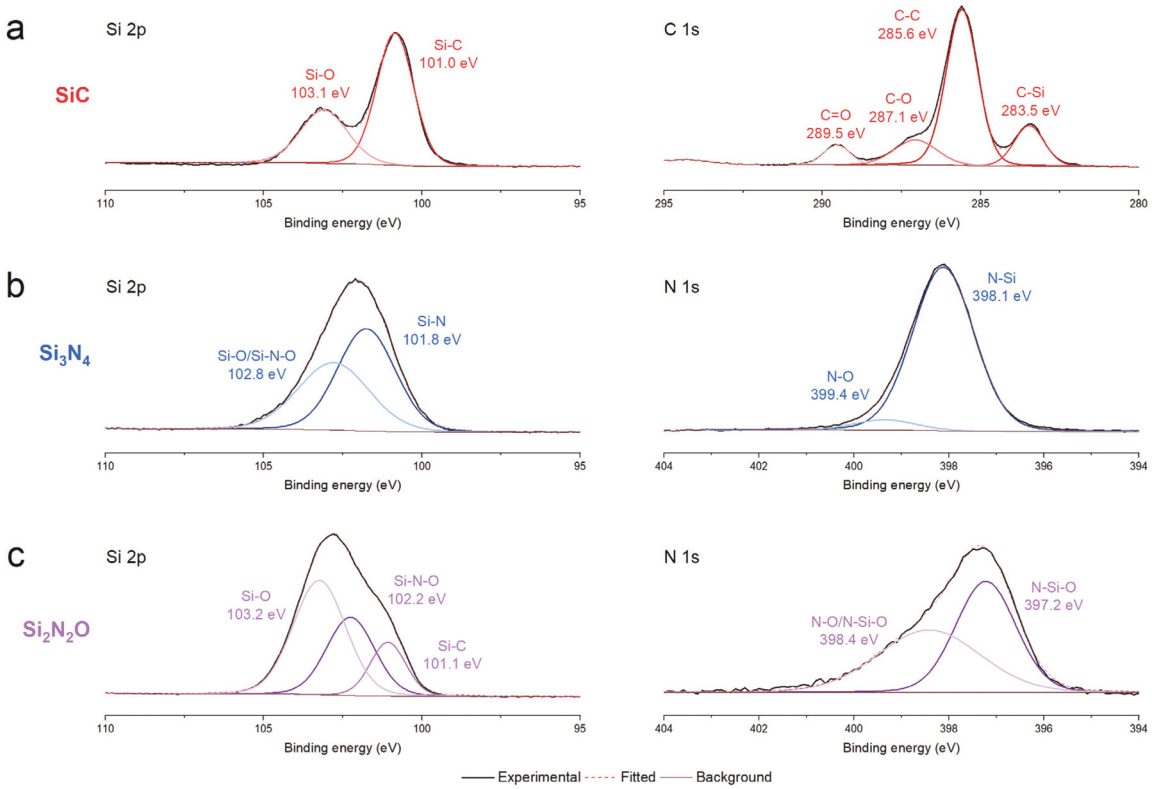

Fig. 6 Representative XPS core-level spectra of (a) SiC, (b) Si_3N_4, and (c) Si_2N_2O composites.

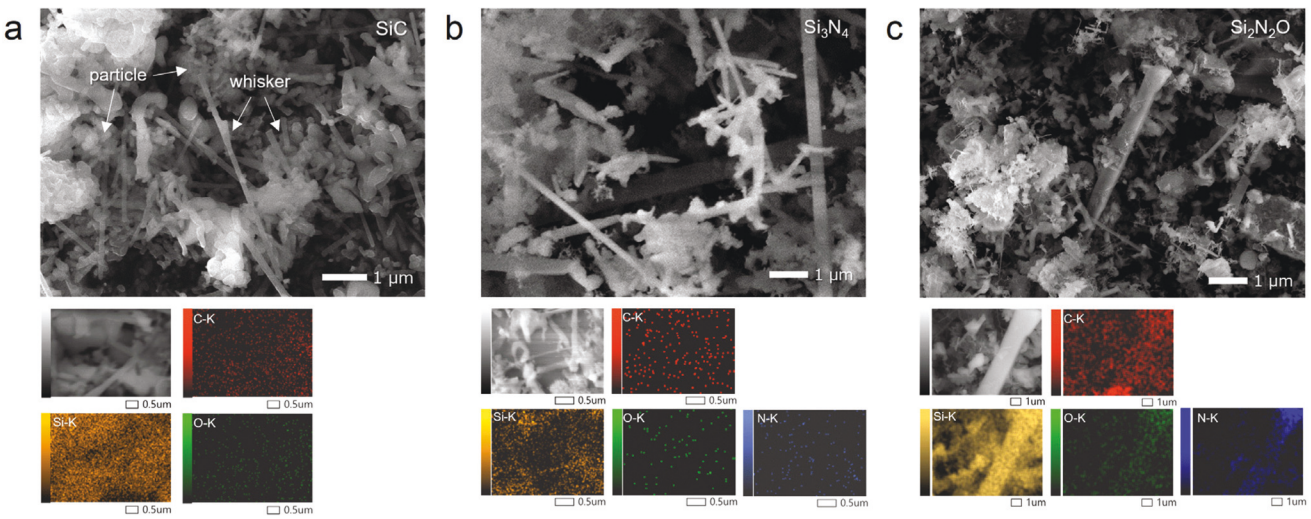

Fig. 7 Representative SEM and EDX images of (a). SiC, (b) Si_3N_4, and (c) Si_2N_2O composites.

areas of SiC from heating at 1450, 1500, and 1600 °C for 8 h are 44, 27, and 10 $m^2\ g^{-1}$, respectively.

BET studies of Si_3N_4 from heating $SDRHA_{60}$ at 1400 and 1500 °C per 8 h/N_2 reveal surface areas of ~20 and ~10 $m^2\ g^{-1}$, respectively. In comparison, Si_3N_4 produced from heating at 1500 °C per 4 h shows an SSA of ~30 $m^2\ g^{-1}$; while Si_2N_2O from heating $SDRHA_{65}$ at 1500 °C per 8 h/95N_2–5H_2 show SSAs of ~10 $m^2\ g^{-1}$. As expected, higher and longer heating temperatures and times result in decreases in specific surface areas, presumably due to the growth and coalescence of fibers and particulates *via* grain-boundary diffusion.[91,95]

The aforementioned studies on composites derived from SDRHA are preludes to investigations using these materials as compatible components in Li^+ energy storage devices. As avail-

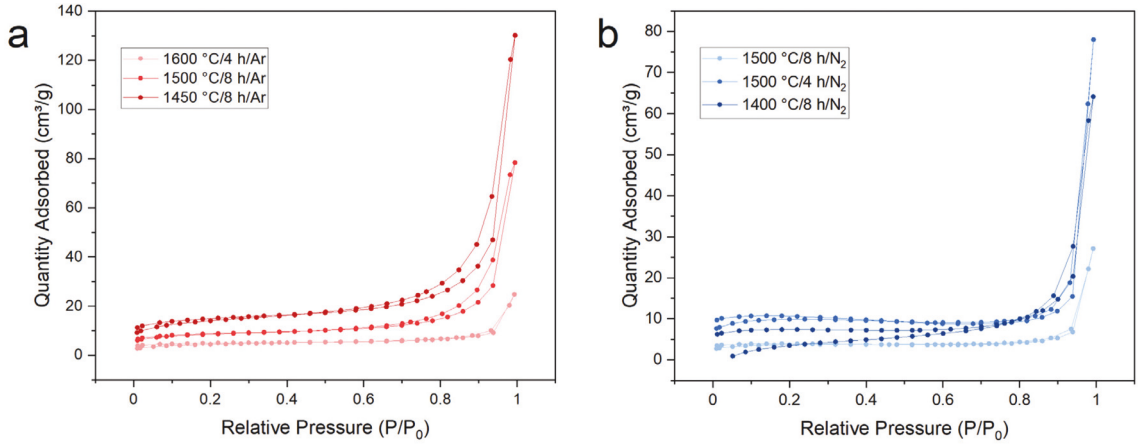

Fig. 8 Representative N_2 adsorption–desorption isotherm plots of (a) SiC and (b) Si_3N_4.

able free surfaces are believed to correlate with charge/discharge kinetics and reversibility, composites with optimized SSAs and appropriate modifications of residual hard carbon contents are in progress.[83,96–100]

Conclusions

SDRHA with adjustable SiO_2 : C ratios makes it an attractive starting material for synthesizing SiC, Si_3N_4, and Si_2N_2O whisker and particle composites. Complete conversion of the SiO_2 in SDRHA to β-SiC was evidenced in samples heated at 1500 °C per 5 h/Ar, while that for α-Si_3N_4 is 1400 °C per 8 h/N_2. On heating under N_2–H_2 mixtures, Si_2N_2O forms as the major crystalline phase (up to 88 wt%). Higher temperatures and longer reaction times enhance SiO_2 reduction but at the expense of BET SSAs, which are desirable for electronic applications and for use in lithium battery applications as will be described in a forthcoming paper.

Likewise, lower SiO_2 : C ratios in SDRHA, *i.e.* more excess carbon in the starting materials facilitate carbothermal reduction at lower temperatures. Amounts of excess free carbon contained in all product composites vary with the SiO_2 : C ratio in the starting SDRHA and heating conditions and can be easily eliminated oxidatively. The absence of metal impurities in the products derived from SDRHA overcomes the long-lasting challenges of generating products with high purities from agricultural wastes, enabling their potential use in various applications.

Conflicts of interest

There are no conflicts to declare.

Acknowledgements

We acknowledge DMR NSF Grant No. DMR-1926199 and a generous gift from Mercedes Benz Research and Development North America (MBRDNA) as support for this work. We also thank the gift of RHA from Wadham Energy Inc., the technical support provided by Michigan Center for Materials Characterization, and Zijing Zhang for the help in studies on Si_2N_2O composites.

References

1 S. S. Hossain, L. Mathur and P. K. Roy, *J. Asian Ceram. Soc.*, 2018, **6**, 299–313.
2 J. G. Lee, P. D. Miller and I. B. Cutler, in *Reactivity of Solids*, ed. J. Wood, O. Lindqvist, C. Helgesson and N.-G. Vannerberg, Springer US, Boston, MA, 1977, pp. 707–711.
3 W.-S. Seo, K. Koumoto and S. Aria, *J. Am. Ceram. Soc.*, 2000, **83**, 2584–2592.
4 M. F. Zawrah, M. A. Zayed and M. R. K. Ali, *J. Hazard. Mater.*, 2012, **227–228**, 250–256.
5 R. Rajarao and V. Sahajwalla, *J. Cleaner Prod.*, 2016, **133**, 1277–1282.
6 Y. L. Chiew and K. Y. Cheong, *J. Mater. Sci. Eng. B*, 2011, **176**, 951–964.
7 A. Selvam, N. G. Nair and P. Singh, *J. Mater. Sci. Lett.*, 1998, **17**, 57–60.
8 S. Maroufi, M. Mayyas and V. Sahajwalla, *ACS Sustainable Chem. Eng.*, 2017, **5**, 4171–4178.
9 S. Maroufi, M. Mayyas and V. Sahajwalla, *J. Cleaner Prod.*, 2017, **157**, 213–221.
10 F. J. Narciso-Romero and F. Rodríguez-Reinoso, *J. Mater. Sci.*, 1996, **31**, 779–784.
11 J. Kuang and W. Cao, *J. Am. Ceram. Soc.*, 2013, **96**, 2877–2880.
12 S.-C. Chiu, H.-C. Yu and Y.-Y. Li, *J. Phys. Chem. C*, 2010, **114**, 1947–1952.
13 C. Real, M. D. Alcalá and J. M. Criado, *J. Am. Ceram. Soc.*, 2004, **87**, 75–78.
14 R. Pode, *Renewable Sustainable Energy Rev.*, 2016, **53**, 1468–1485.

15 Y. Shen, P. Zhao and Q. Shao, *Microporous Mesoporous Mater.*, 2014, **188**, 46–76.
16 M. M. Haslinawati, K. A. Matori, Z. A. Wahab, H. A. A. Sidek and A. T. Zainal, *Int. J. Basic Appl. Sci.*, 2009, **09**(9), 111–114.
17 J. Su, B. Gao, Z. Chen, J. Fu, W. An, X. Peng, X. Zhang, L. Wang, K. Huo and P. K. Chu, *ACS Sustainable Chem. Eng.*, 2016, **4**, 6600–6607.
18 J. Li, T. Shirai and M. Fuji, *J. Ceram. Soc. Jpn.*, 2012, **120**, 338–340.
19 P. Gorthy and M. P. G, *J. Am. Ceram. Soc.*, 1999, **82**, 1393–1400.
20 K. Sujirote and P. Leangsuwan, *J. Mater. Sci.*, 2003, **38**, 4739–4744.
21 Y. Zou and T. Yang, in *Rice Bran and Rice Bran Oil*, ed. L.-Z. Cheong and X. Xu, AOCS Press, 2019, pp. 207–246.
22 B. Singh, in *Waste and Supplementary Cementitious Materials in Concrete*, ed. R. Siddique and P. Cachim, Woodhead Publishing, 2018, pp. 417–460.
23 M. A. Hamad and I. A. Khattab, *Thermochim. Acta*, 1981, **48**, 343–349.
24 V. Vaibhav, U. Vijayalakshmi and S. M. Roopan, *Spectrochim. Acta, Part A*, 2015, **139**, 515–520.
25 A. Yeoh, R. Biden, C. Chong and C. Tay, in *part at the UNIDO/ESCAP/RCTT*, Alor Setar, Malaysia, 1979.
26 C. Hwang and D. Wu, American Concrete Institute, Special publication, online, 1989, pp. 733–765.
27 W. Li, Q. Huang, H. Guo and Y. Hou, *Ceram. Int.*, 2018, **44**, 4500–4503.
28 J. Chen, Q. Kong, Z. Liu, Z. Bi, H. Jia, G. Song, L. Xie, S. Zhang and C.-M. Chen, *ACS Sustainable Chem. Eng.*, 2019, **7**, 19027–19033.
29 A. Ortega, M. D. Alcalá and C. Real, *J. Mater. Process. Technol.*, 2008, **195**, 224–231.
30 N. Wangmooklang, K. Sujirote, S. Jinawath and S. Wada, *J. Eur. Ceram. Soc.*, 2007, **27**, 2111–2117.
31 X. Wan, PhD thesis, The University of New South Wales, 2013.
32 A. Abdulhameed, H. Mbuvi and E. O. Changamu, *J. Water Techol. Treat Methods*, 2018, **1**, 106–110.
33 V. Pavarajarn, R. Precharyutasin and P. Praserthdam, *J. Am. Ceram. Soc.*, 2010, **93**, 973–979.
34 R. V. Krishnarao and M. M. Godkhindi, *Ceram. Int.*, 1992, **18**, 243–249.
35 J. C. Marchal, D. J. Krug, P. McDonnell, K. Sun and R. M. Laine, *Green Chem.*, 2015, **17**, 3931–3940.
36 X. Ma, B. Zhou, W. Gao, Y. Qu, L. Wang, Z. Wang and Y. Zhu, *Powder Technol.*, 2012, **217**, 497–501.
37 U. Kalapathy, A. Proctor and J. Shultz, *Bioresour. Technol.*, 2000, **73**, 257–262.
38 R. M. Laine, J. C. Furgal, P. Doan, D. Pan, V. Popova and X. Zhang, *Angew. Chem.*, 2016, **128**, 1077–1081.
39 X. Zhang, E. Temeche and R. M. Laine, *Green Chem.*, 2020, **22**, 7491–7505.
40 C. D. Li, M. U. Saeed, N. Pan, Z. F. Chen and T. Z. Xu, *Materials Des.*, 2016, **107**, 440–449.
41 E. Temeche, M. Yu and R. M. Laine, *Green Chem.*, 2020, **22**, 4656–4668.
42 R. M. Laine, J. C. Furgal, P. Doan, D. Pan, V. Popova and X. Zhang, *Angew. Chem., Int. Ed.*, 2016, **55**, 1065–1069.
43 L. Bai, Z. F. Karnowo, S. Kudo, K. Norinaga, Y. G. Wang and J. I. Hayashi, *Energy Fuels*, 2014, **28**(11), 7133–7139.
44 A. Chakraverty, P. Mishra and H. D. Banerjee, *J. Mater. Sci.*, 1988, **23**, 21–24.
45 B. K. Padhi and C. Patnaik, *Ceram. Int.*, 1995, **21**, 213–220.
46 G. Ayalasomayajuala, A. Garg, S. Kapila, K. Chandrashekhara and V. Flanigan, International SAMPE Technical Conference, 2004, pp. 2435–2444.
47 M. Thommes, K. Kaneko, A. V. Neimark, J. P. Olivier, F. Rodriguez-Reinoso, J. Rouquerol and K. S. W. Sing, *Pure Appl. Chem.*, 2015, **87**, 1051–1069.
48 A. L. Ortiz, F. Sánchez-Bajo, F. L. Cumbrera and F. Guiberteau, *Mater. Lett.*, 2001, **49**, 137–145.
49 G. Luo, Z. Zhang, J. Hu, J. Zhang, Y. Sun, Q. Shen and L. Zhang, *Materials*, 2020, **13**, 1496.
50 Y. Cui, J. Chen, Y. Di, X. Zhang and W. Lei, *AIP Adv.*, 2017, **7**, 125219.
51 J.-G. Lee and I. B. Cutler, *Am. Ceram. Soc. Bull.*, 1975, **54**, 195–198.
52 B. V. Radhakrishna Bhat and G. P. Sanghi, *Bull. Mater. Sci.*, 1987, **9**, 295–303.
53 J. L. Blumenthal, M. J. Santy and E. A. Burns, *AIAA J.*, 1966, **4**, 1053–1057.
54 C. Y. Chen, C. I. Lin and S. H. Chen, *Br. Ceram. Trans.*, 2000, **99**, 57–62.
55 A. W. Weimer, K. J. Nilsen, G. A. Cochran and R. P. Roach, *AIChE J.*, 1993, **39**, 493–503.
56 V. D. Krstic, *J. Am. Ceram. Soc.*, 1992, **75**, 170–174.
57 N. Klinger, E. L. Strauss and K. L. Komarek, *J. Am. Ceram. Soc.*, 1966, **49**, 369–375.
58 P. D. Miller, J. G. Lee and I. B. Cutler, *J. Am. Ceram. Soc.*, 1979, **62**, 147–149.
59 A. Taylor and D. S. Laidler, *Br. J. Appl. Phys.*, 1950, **1**, 174–181.
60 K. F. Jusnes, M. Tangstad and E. Ringdalen, in *Extraction 2018*, ed. B. R. Davis, M. S. Moats, S. Wang, D. Gregurek, J. Kapusta, T. P. Battle, M. E. Schlesinger, G. R. Alvear Flores, E. Jak, G. Goodall, M. L. Free, E. Asselin, A. Chagnes, D. Dreisinger, M. Jeffrey, J. Lee, G. Miller, J. Petersen, V. S. T. Ciminelli, Q. Xu, R. Molnar, J. Adams, W. Liu, N. Verbaan, J. Goode, I. M. London, G. Azimi, A. Forstner, R. Kappes and T. Bhambhani, Springer International Publishing, Cham, 2018, pp. 717–727.
61 S. s. Cole, *J. Am. Ceram. Soc.*, 1935, **18**, 149–154.
62 A. C. D. Chaklader and A. L. Roberts, *J. Am. Ceram. Soc.*, 1961, **44**, 35–41.
63 J. Li, T. Shirai and M. Fuji, *Adv. Powder Technol.*, 2013, **24**, 838–843.
64 G. Gundiah, G. V. Madhav, A. Govindaraj, M. M. Seikh and C. N. R. Rao, *J. Mater. Chem.*, 2002, **12**, 1606–1611.
65 P. D. Ramesh and K. J. Rao, *J. Mater. Res.*, 1994, **9**, 2330–2340.

66 B. Ma, Z. Huang, L. Mei, M. Fang, Y. Liu, X. Wu and X. Hu, *JOM*, 2016, **68**, 1456–1464.
67 S. W. Yang, S. Y. Shan, W. H. Ma and H. Wang, *Mater. Sci. Forum*, 2011, **675–677**, 175–178.
68 B. Bergman and H. Heping, *J. Eur. Ceram. Soc.*, 1990, **6**, 3–8.
69 X. Li, J. Wang, H. Ji and X. Xu, *Aerosp. Mater. Technol.*, 2016, **42**, 95–98.
70 X. Wan, G. Zhang, O. Ostrovski and H. Aral, *in part at the Thirteenth International Ferroalloys Congress: Efficient Technologies in Ferroalloy Industry*, Karaganda, Kazakhstan, 2013.
71 F. Yan, Y. D. Zheng, P. Chen, L. Sun and S. L. Gu, *Opt. Mater.*, 2003, **23**, 113–116.
72 A. Parrillo, G. Sánchez and A. B. Alles, *SN Appl. Sci.*, 2021, **3**, 268.
73 K. R. Carduner, S. S. Shinozaki, M. J. Rokosz, C. R. Peters and T. J. Whalen, *J. Am. Ceram. Soc.*, 1990, **73**, 2281–2286.
74 *Pergamon Materials Series*, ed. K. J. D. MacKenzie and M. E. Smith, Pergamon, 2002, vol. 6, pp. 201–268.
75 K. J. D. MacKenzie, *Solid State Ionics*, 2004, **172**, 383–388.
76 P. J. Baxter, C. Bonadonna, R. Dupree, V. L. Hards, S. C. Kohn, M. D. Murphy, A. Nichols, R. A. Nicholson, G. Norton, A. Searl, R. S. J. Sparks and B. P. Vickers, *Science*, 1999, **283**, 1142–1145.
77 D. G. Nair, A. Fraaij, A. A. K. Klaassen and A. P. M. Kentgens, *Cem. Concr. Res.*, 2008, **38**, 861–869.
78 R. Ghita, C. Logofatu, C.-C. Negrila, F. Ungureanu, C. Cotirlan, A.-S. Manea, M.-F. Lazarescu and C. Ghica, in *Crystalline Silicon - Properties and Uses*, ed. S. Basu, IntechOpen, 2011.
79 T. N. Taylor, *J. Mater. Res.*, 1989, **4**, 189–203.
80 K.-H. Lee, S.-K. Lee and K.-S. Jeon, *Appl. Surf. Sci.*, 2009, **255**, 4414–4420.
81 M. Grodzicki, R. Wasielewski, S. A. Surma and A. Ciszewski, *Acta Phys. Pol., A*, 2009, **116**, 4.
82 H. A. Bland, E. L. H. Thomas, G. M. Klemencic, S. Mandal, D. J. Morgan, A. Papageorgiou, T. G. Jones and O. A. Williams, *Sci. Rep.*, 2019, **9**, 2911.
83 Z. Zhu, F. Liang, Z. Zhou, X. Zeng, D. Wang, P. Dong, J. Zhao, S. Sun, Y. Zhang and X. Li, *J. Mater. Chem. A*, 2018, **6**, 1513–1522.
84 Y. Zhu, M. Chen, Q. Li, C. Yuan and C. Wang, *Carbon*, 2017, **123**, 727–734.
85 E. Bódis, I. Cora, P. Németh, O. Tapasztó, M. Mohai, S. Tóth, Z. Károly and J. Szépvölgyi, *Ceram. Int.*, 2019, **45**, 4810–4816.
86 G.-R. Yang, Y.-P. Zhao, Y. Z. Hu, T. Paul Chow and R. J. Gutmann, *Thin Solid Films*, 1998, **333**, 219–223.
87 S. M. Castanho and R. Moreno, *Cerâmica*, 1998, **44**, 141–145.
88 X. Sun, H. T. Liu and H. F. Cheng, *RSC Adv.*, 2017, **7**, 47833–47839.
89 X. Hu, C. Shao, J. Wang and H. Wang, *J. Mater. Sci.*, 2017, **52**, 7555–7566.
90 C. Zou, C. Zhang, B. Li, S. Wang, Z. Xie and Y. Song, *Mater. Sci. Eng., A*, 2015, **620**, 420–427.
91 S. Maro, M. Mayyas and V. Sahajwalla, *J. Cleaner Prod.*, 2017, **157**, 213–221.
92 J. V. Milewski, F. D. Gac, J. J. Petrovic and S. R. Skaggs, *J. Mater. Sci.*, 1985, **20**, 1160–1166.
93 A. Chrysanthou, P. Grieveson and A. Jha, *J. Mater. Sci.*, 1991, **26**, 3463–3476.
94 Y. Li, Q. Wang, H. Fan, S. Sang, Y. Li and L. Zhao, *Ceram. Int.*, 2014, **40**, 1481–1488.
95 X. K. Li, L. Liu, Y. X. Zhang, Sh. D. Shen, S. Ge and L. C. Ling, *Carbon*, 2001, **39**, 159–165.
96 F. Béguin, F. Chevallier, C. Vix-Guterl, S. Saadallah, V. Bertagna, J. N. Rouzaud and E. Frackowiak, *Carbon*, 2005, **43**, 2160–2167.
97 H. Zheng, Q. Qu, L. Zhang, G. Liu and V. S. Battaglia, *RSC Adv.*, 2012, **2**, 4904–4912.
98 H. Fujimoto, K. Tokumitsu, A. Mabuchi, N. Chinnasamy and T. Kasuh, *J. Power Sources*, 2010, **195**, 7452–7456.
99 G. Li, O. Ting, T. Xiong, Z. Jiang, D. Adekoya, Y. Wu, Y. Huang and M. S. Balogun, *Carbon*, 2021, **174**, 1–9.
100 K. Ye, K. Li, Y. Lu, Z. Guo, N. Ni, H. Liu, Y. Huang, H. Ji and P. Wang, *TrAC, Trends Anal. Chem.*, 2019, **116**, 102–108.

